ISBN: 978-3-95450-194-6 doi:10.18429/JACoW-LINAC2018-MO2A03

TECHNOLOGY DEVELOPMENTS OF ELI-NP GAMMA BEAM SYSTEM

L. Piersanti*, D. Alesini, A. Battisti, M. Bellaveglia, S. Bini, F. Cardelli, R. Di Raddo, A. Falone, A. Gallo, V. Lollo, L. Pellegrino, S. Pioli, S. Tomassini, A. Variola INFN-LNF, Frascati, Italy
L. Ficcadenti, M. Migliorati[1], A. Mostacci[1], L. Palumbo[1], V. Pettinacci INFN-Roma, Rome, Italy
D. T. Palmer, L. Serafini INFN-Sezione di Milano
K. Cassou, D. Douillet, K. Dupraz, T. Le Barillec, A. Martens, C. F. Ndiaye, Y. Peinaud, F. Zomer LAL, CNRS/IN2P3 Université Paris Sud - France
N. Beaugerard, B. Lacrampe, H. Rocipon, ALSYOM/SEIV-ALCEN, France
[1]also at Sapienza University of Rome, SBAI Department Rome, Italy

Abstract

The ELI-NP gamma beam system (GBS) is a linac based gamma-source in construction in Magurele (RO) by the European consortium EuroGammaS led by INFN. Photons with tunable energy, from 0.2 to 19.5 MeV, and with intensity and brilliance beyond the state of the art, will be produced by Compton back-scattering between a high quality electron beam (up to 740 MeV) and an intense laser pulse at 100 Hz repetition rate. Production of very intense photon flux with narrow bandwidth requires multi-bunch operation and laser recirculation at the interaction point. In this paper, the main technological developments carried out by the EuroGammaS consortium for the generation of the ELI-NP gamma beam will be described with a special emphasis on the electron linac technology, such as: RF-gun and C-band accelerating structures design fabrication and tests; low level RF (LLRF) and synchronization systems specifications and development. Finally, the laser recirculation apparatus design is briefly described and first results reported.

INTRODUCTION

An advanced source of gamma-ray photons will be built in Magurele in the framework of the ELI-NP project [1, 2] by the EuroGammaS consortium. The gamma-rays will be generated by a high quality electron beam colliding with a high power laser pulse (200 mJ, 3.5 ps, 515 nm) recirculated 32 times at the interaction point. The machine is expected to produce photons with tunable energy between 0.2 and 19.5 MeV with a narrow bandwidth (< 0.5 %) and a high spectral density ($0.8\text{-}4 \times 10^4$ ph/s eV) [3].

The accelerator layout is based on a C-band (5712 MHz) RF linac, with a S-band (2856 MHz) photo-injector similar to that of SPARC_LAB at LNF-INFN (Frascati, Italy) [4], able to deliver a high phase space density electron beam in the 300-740 MeV energy range. The repetition rate is 100 Hz and, in order to reach the required photon flux, the machine is foreseen to work in multi-bunch mode (fitting 32 electron bunches spaced by 16 ns in each RF pulse), thus with an effective repetition rate of 3.2 kHz. The main electron beam parameters of the ELI-NP-GBS, together with the description of the complete RF system have been reported in [2, 5].

* luca.piersanti@lnf.infn.it

LINAC OVERVIEW

ELI-NP-GBS photo-injector comprises a 1.6 cell S-band RF-gun, which has been manufactured with a new fabrication technique which does not require copper brazing [6–9], and two S-band 3 m long SLAC-type TW constant gradient accelerating structures. The S-band system comprises also two deflecting cavities used for longitudinal beam diagnostics. The linac booster is made of 12 travelling wave (TW) C-band disk loaded accelerating structures. Moreover, a waveguide high order mode (HOM) damping system that employs 4 SiC RF absorbers for each cell [10–13] has been included in the design, to avoid beam break up instabilities that may arise due to multi-bunch operation.

In order to reduce bunch-by-bunch energy spread due to structure beam loading (BL), a tailored pulse shaping compensation has to be provided to the klystrons by the LLRF systems [5]. Moreover, since the use of pulse compressors would make the pulse shaping even more critical, each accelerating section is individually driven by a dedicated power station (with the exception of the last 4 TW sections that are fed by 2 klystrons). A sketch of the linac has been reported in Figure 1.

S-BAND RF-GUN DESIGN, LOW AND HIGH POWER TESTS

RF photo-guns find several type of applications including high brightness electron sources for free-electron lasers, energy recovery linacs, Compton/Thomson photon sources. Being the achievable beam brightness proportional to the peak field at the cathode, in the last generation of RF guns a great effort has been put to increase the field amplitude while reducing, at the same time, the breakdown phenomena. Moreover, modern RF guns must be able to withstand high repetition rate operation (of the order of 100 Hz) with a reasonable realization cost. Currently the standard fabrication process relies on copper brazing. However, this technique requires large vacuum furnaces, it is expensive and has a non-negligible risk of failure. Furthermore, studies carried out on X-band prototypes indicated that it is possible to reduce the breakdown probability if copper thermal stress is avoided [14]. For all these reasons, a new brazing-free fabrication method based on the use of special RF-vacuum gaskets has been recently developed at LNF-INFN [7], and

Content from this work may be used under the terms of the CC BY 3.0 licence (© 2018). Any distribution of this work must maintain attribution to the author(s), title of the work, publisher, and DOI.

ISBN: 978-3-95450-194-6 doi:10.18429/JACoW-LINAC2018-MO2A03

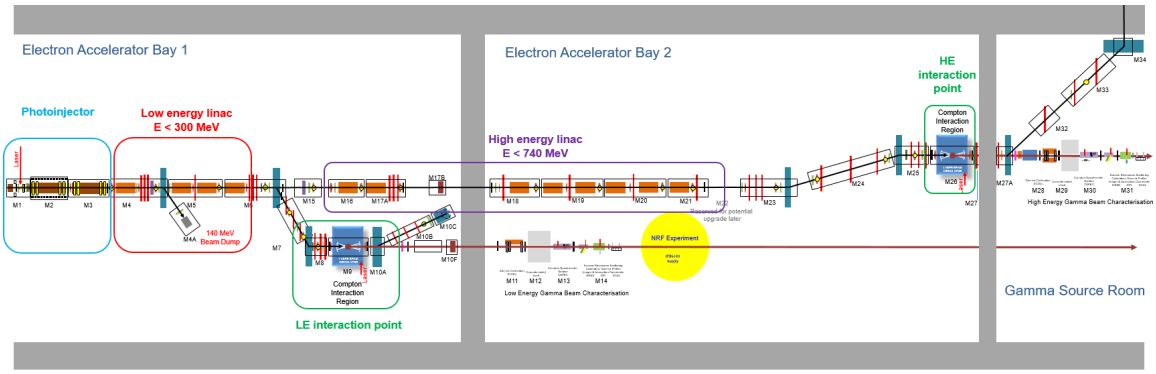

Figure 1: ELI-NP GBS linac overview.

successfully applied to the realization of a first RF gun prototype [6, 15–17]. The same technique has also been adopted for the realization of the 1.6 cell S-band ELI-NP-GBS RF gun.

Electromagnetic Design

The electromagnetic design of the gun has been performed using 2D and 3D codes (Poisson Superfish [18] and ANSYS Electronics [19]). The iris profile, with an elliptical shape and a large aperture, simultaneously reduces the peak surface electric field, increases the frequency separation between the two resonant modes and improves the pumping efficiency on the half-cell. The coupling window between the rectangular waveguide and the full cell has been strongly rounded to reduce the peak surface magnetic field and, consequently, the pulsed heating [6, 20]. To compensate the dipole field component, induced by the presence of the coupling hole in the full cell, a symmetric port (connected to a circular pipe below cut off) has been included in the gun [21–23] and is used as vacuum pumping port. The RF-gun main parameters have been reported in Table 1.

Table 1: ELI-NP-GBS RF-gun Design Parameters

Parameter	Value
Resonant frequency (f_{res})	2856 MHz
Cathode peak field (E_{cath})	120 MVm
Filling time (τ)	410 ns
Quality factor (Q_0)	14 600
Coupling coefficient (β)	3
Total RF pulse length	1.5 µs
Shunt impedance (R)	1.64 MΩ
Frequency separation $0/\pi$ mode	41.5 MHz
Pulsed heating	< 36 °C
Average dissipated power	1.3 kW

The operation at 100 Hz with 1.5 µs RF pulses results in an average dissipated power into the structure larger than 1 kW. To avoid detuning during operation, a careful design of the cooling system has been performed. The gun has 6 cooling channels: three for the full cell, one for the iris, one for the half cell and one for the cathode. The fully coupled thermal, structural and electromagnetic analysis, has been carried out by means of ANSYS Workbench [19]. The final temperature distribution at regime has been calculated and corresponds to a deformation of few microns. As far as the electromagnetic design is concerned, the expected frequency detuning of the gun during operation is lower than 100 kHz and the field flatness perturbation is completely negligible. Such detuning can be compensated changing the water inlet temperature of about 2 °C .

RF-Gun Manufacturing

The body of the gun has been fabricated from a single piece of OFHC copper using diamond tools. The rounded coupler geometry and the overall gun body have been realized with a 5 axis milling machine. The full cell has then been sealed clamping the body with the pipe by means of the special gasket [7, 9], that simultaneously guarantees the RF contact and the vacuum seal, avoiding sharp edges and gaps. The RF gun has been manufactured by COMEB [24] with a precision on the internal dimensions of ≈10 µm and surface roughness lower than 150 nm. The cathode has been realized from a single piece of copper and has been clamped to the structure. The RF contact between the cathode and the gun body is guaranteed by pressure, while the vacuum seal by a special aluminum gasket not exposed to RF. The cathode dissipates around 200 W, thus it has to be cooled independently. Before the final clamping, the gun has been cleaned with ALMECO-19 detergent in an ultra-sound bath.

Low and High Power Tests

Low power RF test and tuning of the gun have been performed with the bead drop technique [25], measuring the reflection coefficient with a Network Analyzer. The tuning has been done by means of deformation tuners placed in the full cell. The resulting measured coupling coefficient was $\beta = 2.64$ in fair agreement with the design value, while all other parameters were in very good agreement with the ones reported in Table 1.

High power RF tests have been performed at Bonn University in collaboration with Research Instruments [26]. The power source employed was the ELI-NP-GBS Scandinova RF unit based on a solid state modulator (K2-3) and 60 MW

Content from this work may be used under the terms of the CC BY 3.0 licence (© 2018). Any distribution of this work must maintain attribution to the author(s), title of the work, publisher, and DOI.

ISBN: 978-3-95450-194-6 doi:10.18429/JACoW-LINAC2018-MO2A03

S-band Toshiba klystron. The aim of the test was to achieve 120 MV/m at the cathode (corresponding to 14 MW input power) at the nominal repetition rate and RF pulse duration. The klystron power, repetition rate and pulse length were progressively increased, while breakdown phenomena were detected looking at the ion pumps current absorption and RF signals from pickups. The modulator HV interlock conditions were: (a) ion pumps current absorption exceeding a pressure of 5×10^{-8} mbar; (b) high reflected power towards the klystron; (c) distortions of the reflected signal due to breakdown phenomena. The RF conditioning lasted about 160 hours and the gun reached the nominal parameters with a breakdown rate (BDR) of few 1×10^{-5} bpp. Since the BDR trend was constantly decreasing, and considering the test stand limited time availability, the test has been considered successful. At the end of conditioning and without power the vacuum pressure in the gun was lower than 5×10^{-10} mbar.

C-BAND STRUCTURES DESIGN, TUNING AND HIGH POWER TESTS

ELI-NP-GBS booster linac consists of 12 TW C-Band disk loaded accelerating sections. Each section is 1.8 m long, quasi-constant gradient with a $2\pi/3$ field phase advance per cell and will operate at an average accelerating gradient of 33 MV/m. Since the linac operation is multi-bunch, the structures have been designed with an effective damping of the cell dipole HOM based on waveguide coupled to SiC absorbers. The design criteria together with the main structure parameters have been thoroughly illustrated in [13]. The HOM damping system is similar to the one adopted for the CLIC X-band structures [27], but the mechanical design has been strongly simplified in order to reduce the cost and to ease the manufacturing. Each cell has four waveguides that allow the excited HOMs to propagate and dissipate into RF absorbers. A dedicated study performed on a single 12-cell module to assess the effectiveness of the SiC absorbers can be found in [13]. The input and output couplers have two symmetric ports and race track cell geometries to minimize the dipole and quadrupole field components introduced by the coupling holes. The input coupler integrates also a splitter that allows a symmetric RF feeding of the structure, while the output one has two symmetric ports connected to two RF loads.

Structure Fabrication

In order to have a better control of the brazing process, each structure has been conceived in 10 separate modules, which have been individually realized, brazed and vacuum tested: the input and output couplers (including two adjacent cells) plus eight 12-cell modules. The manufacturing of the cells required several steps. After a rough machining, the cells underwent a stress relieving treatment in a vacuum furnace. Then, they have been milled, while the final machining of the irises has been performed by means of the ultra-precise lathe Schaublin 225 TM-CNC that guarantees a precision ±5 µm and a surface roughness lower than 50 nm. Each cell includes also four deformation tuners and eight cooling pipes, needed to withstand the 100 Hz operation. The manufacturing of the input and output couplers followed a similar procedure. All components have been then cleaned in several steps in an ultrasound bath. After brazing a vacuum test with a sensitivity lower than 5×10^{-10} mbar/l/s has been carried out. The SiC (Ekasic-P) absorbers tiles (pre-machined) have then been inserted in the modules and the whole structure was assembled together and brazed. After the final brazing, performed at INFN Legnaro National Laboratories, and a moderate bake-out at 100 °C, a leak test has been performed with a sensitivity lower than 5×10^{-10} mbar/l/s. A pressure of few 1×10^{-9} mbar has been reached with just one ion pump connected on one side.

Low and High Power Tests

Eight structures have been tuned at LNF so far, measuring the scattering parameters at the input and output ports with a network analyzer. The magnitude of the accelerating field and the phase advance per cell have been evaluated with the bead pull technique, using a metallic sphere as perturbing object. The tuning has been done acting on the four deformation tuners of each cell, using the same procedure illustrated in [28–30]. The field flatness, the phase advance and the cumulative phase advance after the tuning procedure were the nominal ones for all the fabricated structures. As example, the calculated field flatness of structure number 6 is below 1%, the phase advance per cell is within ±2 deg, while the cumulative phase advance error is limited within ±5 deg. At the resonant frequency the reflection coefficient at the input port is lower than −25 dB, while the transmission coefficient between input and output port is ≈−8.5 dB, i.e. in good agreement with the designed total attenuation.

The first prototype structure has also been tested at high power at the Bonn University under the responsibility of Research Instruments. The power source was one of the ELI-NP-GBS C-band station, i.e. a Scandinova RF unit based on K2-2 solid state modulator adapted for 50 MW C-band Toshiba klystron (E37212). The aim of the RF conditioning was to reach the nominal power at the input coupler (40 MW), repetition rate (100 Hz) and pulse length (820 ns). The klystron power, repetition rate and pulse length were progressively increased following the same procedure reported in the previous section for the RF-gun. The RF conditioning was successfully completed after 190 hours. The vacuum pressure, measured both at the beginning and at the end of the structure, was of the order of 1×10^{-8} mbar. The BDR at the end of the conditioning was of the order of few 1×10^{-6} bpp/m.

LLRF AND SYNCHRONIZATION SYSTEMS

LLRF System

The LLRF system for the ELI-NP-GBS (Libera LLRF) has been developed by Instrumentation Technologies [31]

Content from this work may be used under the terms of the CC BY 3.0 licence (© 2018). Any distribution of this work must maintain attribution to the author(s), title of the work, publisher, and DOI.

ISBN: 978-3-95450-194-6 doi:10.18429/JACoW-LINAC2018-MO2A03

Content from this work may be used under the terms of the CC BY 3.0 licence (© 2018). Any distribution of this work must maintain attribution to the author(s), title of the work, publisher, and DOI.

and consists of 13 temperature stabilized boards (one dedicated to each power unit): 3 S-band and 10 C-band. This choice has been made in order to guarantee the maximum flexibility in terms of pulse shaping and machine operation stability. One of the main features of Libera LLRF platform is, in fact, the possibility to perform a pulse-by-pulse feedback. Moreover, the pulse shape can be arbitrarily set (e.g. for BL compensation) simply loading a user defined mask to Libera FPGA. The request for thermal stabilization has been introduced to compensate the long-term effect of temperature drifts, that must not exceed 100 fs for normal operation: (24 ± 2) °C. Overall Libera LLRF modules have to guarantee an amplitude resolution of 0.1 % RMS and a phase added jitter lower than 10 fs. Each board contains four main elements: (i) the temperature stabilized analog front-end,(ii) the analog back-end (with 1 RF vector modulator), (iii) the main CPU (which hosts the sampling cards, the FPGA and the EPICS control system server), and (iv) the LO generator and timing unit. The main parameters of Libera LLRF together with some preliminary measurements performed at LNF have been reported in [32].

Synchronization System

The general ELI-NP-GBS synchronization requirement is that the relative arrival time jitter of the electron bunches and laser pulses has to be lower than 500 fs rms at the interaction point (IP). For this reason, the synchronization system has been designed to provide to all clients an ultra-stable reference with a relative jitter < 70 fs. Given the significant link lengths, the reference will be distributed with optic fibers (very low attenuation over hundreds of meters, larger sensitivity obtainable by optical based timing detection). The ELI-NP-GBS synchronization system has been manufactured by Menlo Systems [33] and it consists of two main parts: reference generation and distribution, client synchronization. The reference signal is provided by a Reference Master Oscillator (RMO) which is a μ-wave crystal oscillator (MO-2856-V3 produced by Laurin A.G.) with ultra-low phase noise (10 Hz-10 MHz measured absolute jitter < 60 fs). The RMO provides a stable reference tone to Menlo Optical Master Oscillator (OMO), which is a Er-doped mode-locked laser oscillator, that encodes the reference timing information in the repetition rate of short optical pulses at 1560 nm. Using such configuration, the RMO guarantees the long term stability of the OMO, and imprints its low-frequency noise figure to the whole facility timing.

Once the laser pulses are generated, they are amplified and distributed to all the clients. One of the channels is further amplified and converted by a second harmonic generator to a 780 nm free space output, used as direct seed for the photocathode laser system. Four main clients have been identified in the ELI-NP-GBS machine: two interaction lasers and two RF extractors (one at 2856 MHz and one at 5712 MHz) that provide the RF reference to the LLRF systems and power units. Depending on the nature of the clients, the PLL can be either “fully optical” (employing optical cross-correlators), or “electro-optical” locking the RF-extractor to a μ-wave VCO. The clients will be reached by means of four dispersion compensated fiber links with active length stabilization, in order to deliver short (< 200 fs) synchronous pulses to the end users. The active length stabilization is achieved sending back a fraction of pulse from the link-end and comparing it to a reference pulse near the oscillator. A full description of the synchronization system has been reported in [32].

LASER BEAM CIRCULATOR

The IP laser architecture is based on a chirped-pulse amplification scheme, composed of an Yb oscillator (20 nJ, 62 MHz, 200 fs, 1030 nm), a stretcher, several amplifier stages (regenerative + cryo-cooled 350 mJ, 100 Hz), and a compressor. Finally the pulses are frequency doubled in a second harmonic conversion stage to reach the IP specifications (200 mJ, 100 Hz, 3.5 ps, 515 nm).

To optimize the γ-ray beam quality, the optical system at the IP must preserve laser spectral bandwidth while maximizing its flux. The effective increase of the laser beam power at the Compton IP can be obtained with two types of optical systems, namely a Fabry-Perot resonator [34] or an optical recirculator [35–37]. Since the ELI-NP-GBS linac operates in multi-bunch at 100 Hz, a passive optical device able to recirculate and focus several times a single laser pulse at the IP is the optimal solution to maximize the γ flux. As already mentioned, this system must assure a minimal variation of the γ-ray central spectral line. This can be obtained by keeping a constant collision angle (Φ) between laser and electron beam. Furthermore, it is also important to preserve polarization and quality of the wave front. The working principle of the proposed laser beam circulator (LBC) is illustrated in Figure 2: two confocal concave mirrors reflect a circulating Gaussian beam [8] back and forth by forcing it to cross the electron beam axis (i.e., the z axis) at the focus point (the IP). The sequence of lenses equivalent to a "round-trip" is also shown in Figure 2. With a proper choice of the mirror radii of curvature it is possible to alternate beam focusing and collimation.

The final geometry chosen is the so-called "dragon-shape" recirculator depicted in Figure 3. The LBC is made of two big confocal parabolic reflectors, to preserve the quality of the wave front after each pass. Since the crossing angle must be kept constant, the laser-electron beams interaction plane must rotate if more than two recirculations are foreseen. Therefore, a series of two parallel flat mirrors are used to switch from one interaction plane to the next one, while keeping the optical axis parallel to the z axis. Such a pair of parallel mirrors forms an optical invariant providing an emerging beam parallel to the entrance independently of its orientation. Then, the recirculating laser beam axis is always parallel to the symmetry axis z when impinging the parabolic reflectors. By construction, as shown in Figure 3, the mirror-pairs systems are located on a circular helix. It is important to remark that the IP positions is fixed for all laser passes.

ISBN: 978-3-95450-194-6 doi:10.18429/JACoW-LINAC2018-MO2A03

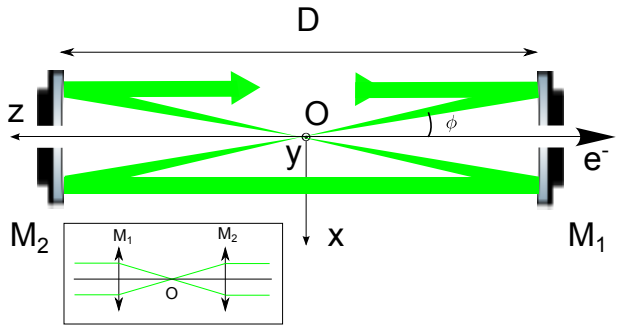

Figure 2: Illustration of the planar confocal recirculator working principle and its equivalent sequence of lenses.

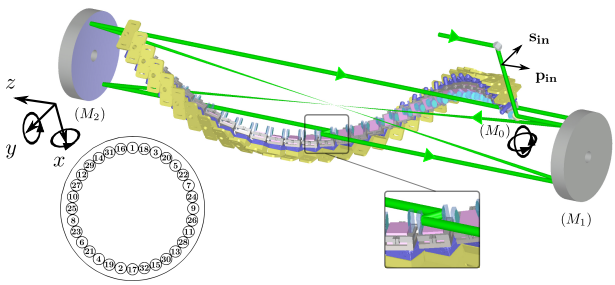

Figure 3: Schematic view of ELI-NP-GBS LBC. The mirror M0 is used to inject the incident laser beam. The 7 degrees of freedom for the mirror motions are sketched: two tilts for M0; two tilts and three translations for M2. Finally the bottom left scheme shows the optical pass ordering.

The time structure of the electron bunch train is strongly related to the RF frequency of the accelerating cavities. Thus, the laser pulse round-trip period must be tightly matched to the bunch repetition frequency. However, since the LBC round-trip lengths are fixed by the parabolic mirrors radius of curvature, the only way to adjust the round-trip path is to rotate the mirror pair system around its own axis. The rotation, in fact, changes the incident angle on the mirrors and consequently the laser optical path length. Moreover, this change is made without modifying the laser beam direction, as it is independent of the mirror pair orientation. Therefore, in order to adjust the timing of each optical recirculation independently, a mirror pair must be placed before each IP crossing. In order to asses the optical alignment of the LBC, a robust optical estimator must be defined. The simplest solution is the intersection point $\{x_n; y_n\}$ of the nth optical pass with the plane $z = 0$ (i.e., the IP). Measurements of $\{x_n; y_n\}$ can be performed inserting a thin pellicle at the LBC center and using an ultrafast CCD. Since the exact position of the electron beam axis with respect to $\{x_n; y_n\}$ cannot be known in advance, the Transverse Distance between the n-th intersection point and the Barycenter (TDB) of all 32 intersection points can be defined instead:

$$TDB_n = \left[\left(x_n - \frac{1}{32} \sum_{i=1}^{32} x_i \right)^2 + \left(y_n - \frac{1}{32} \sum_{i=1}^{32} y_i \right)^2 \right]^{1/2}$$

The alignment system will also be used for the synchronization: adding a second laser pulse train, whose repetition frequency is the same of the electron bunch train, with the same pellicle it is possible to generate an interference pattern which provides information on the relative delay between the two pulses. From previous simulations, the insertion of the pellicle induces a cumulative time delay below 90 fs. This method has the great advantage that only a single pellicle for alignment and synchronization is used, moreover, such solution can monitor online the performance of the LBC, since it is a non-intercepting beam diagnostic element. A detailed description of the LBC design, tolerance and error studies, simulations and some preliminary test results can be found in [38, 39]. The commissioning of the first LBC started in November 2017 in the clean assembly area (PUPS) of ALSYOM [40] (Bordeaux), and it has been carried out by a joint effort of LAL/CNRS and ALSYOM people. A low power circulating laser pulse has been focalized 32 times at the IP with a laser spot waist of (27 ± 2) µm over 32 passes, a TDB lower than 10 µm and synchronized to an external optical reference with time precision of less than 160 fs in air with a transmission of (84 ± 3) % (theoretical 87.5 %). The enhancement factor obtained is 25.6 times the input laser power. The measured values are fully compliant to ELI-NP-GBS specifications.

CONCLUSIONS

In this paper, some of the most relevant technology developments carried out for the ELI-NP-GBS project have been introduced. In particular, an optimization of a 1.6 cell BNL/SLAC/UCLA SW RF gun realized with a brazing-free fabrication technique, the design and realization of HOM damped TW C-band structures and the IP laser recirculation system have been presented. The discussion is also integrated with a brief overview of the LLRF and synchronization systems. All the presented devices have been successfully tested and their installation and commissioning is foreseen in the next future in Magurele.

REFERENCES

[1] O. Adriani *et al.*, "Technical Design Report EuroGammaS proposal for the ELI-NP Gamma beam System", arXiv:1407.3669, 2014.

[2] A. Giribono *et al.*, "ELI-NP GBS Status", in *Proc. IPAC'17*, Copenhagen, Denmark, 2017, pp. 880–883. doi:10.18429/JACoW-IPAC2017-MOPVA016

[3] C. Vaccarezza *et al.*, "Optimization studies for the Beam Dynamics in the RF linac of the ELI-NP Gamma Beam System", in *Proc. IPAC'16*, Busan, Korea, 2016, pp. 1850–1853. doi:10.18429/JACoW-IPAC2016-TUPOW041

[4] M. Ferrario *et al.*, "Experimental Demonstration of Emittance Compensation with Velocity Bunching", *Phy. Rev. Lett.*, vol. 104, no. 5, p. 054801, 2010.

[5] L. Piersanti *et al.*, "The RF system of the ELI-NP gamma beam source", in *Proc. 7th Int. Particle Accelerator Conf. (IPAC'16)*, Busan, Korea, 2016, pp. 407–410. doi:10.18429/JACoW-IPAC2016-MOPMW006

Content from this work may be used under the terms of the CC BY 3.0 licence (© 2018). Any distribution of this work must maintain attribution to the author(s), title of the work, publisher, and DOI.

ISBN: 978-3-95450-194-6 doi:10.18429/JACoW-LINAC2018-MO2A03

Content from this work may be used under the terms of the CC BY 3.0 licence (© 2018). Any distribution of this work must maintain attribution to the author(s), title of the work, publisher, and DOI.

[6] D. Alesini *et al.*, "New technology based on clamping for high gradient radio frequency photogun", *Phys. Rev. ST Accel. Beams*, vol. 18, no. 9, p.092001, 2015.

[7] D. Alesini *et al.*, "Process for manufacturing a vacuum and radio-frequency metal gasket and structure incorporating it", International patent application PCT/IB2016/051464.

[8] F. Cardelli *et al.*, "Design of linac with the new gasket-clamping fabrication technique", in *Proc. 7th Int. Particle Accelerator Conf. (IPAC'16)*, Busan, Korea, 2016, pp. 403–406. doi:10.18429/JACoW-IPAC2016-MOPMW005

[9] D. Alesini *et al.*, "High power test results of the ELI-NP S-band gun fabricated with the new clamping technology without brazing", in *Proc. IPAC'17*, Copenhagen, Denmark, 2017, pp. 3662–3665. doi:10.18429/JACoW-IPAC2017-THOBB1

[10] D. Alesini *et al.*, "The damped C-band RF structures for the European ELI-NP proposal", in *Proc. 4th Int. Particle Accelerator Conf. (IPAC'13)*, Shanghai, China, 2013, pp. 2726–2728.

[11] D. Alesini *et al.*, "Design and RF test of damped C-band accelerating structures for the ELI-NP linac", in *Proc. IPAC'14*, Dresden, Germany, 2014, pp. 3856–3859. doi:10.18429/JACoW-IPAC2014-THPRI042

[12] D. Alesini *et al.*, "Realization and high power tests of damped C-band accelerating structures for the ELI-NP linac", in *Proc. IPAC'16*, Busan, Korea, 2016, pp. 399–402. doi:10.18429/JACoW-IPAC2016-MOPMW004

[13] D. Alesini *et al.*, "Design of high gradient, high repetition rate damped C-band rf structures", *Phys. Rev. Accel. Beams*, vol. 20, no. 3, p. 032004, 2017. doi:10.1103/PhysRevAccelBeams.20.032004

[14] V. Dolgashev *et al.*, "Status of high power tests of normal conducting single-cell standing wave structures", in *Proc. 1st Int. Particle Accelerator Conf. (IPAC'10)*, Kyoto, Japan, 2010, pp. 3810–3812.

[15] D. Cesar *et al.*, "Demonstration of single-shot picosecond time-resolved MeV ilectron imaging using a compact permanent magnet quadrupole based lens", *Phys. Rev. Lett.*, vol. 117, no. 2, p. 024801, 2016. doi:10.1103/PhysRevLett.117.024801

[16] J. Maxson *et al.*, "Direct measurement of sub-10 fs relativistic electron beams with ultralow emittance", *Phys. Rev. Lett.*, vol. 118, no. 15, p. 154802, 2017. doi:10.1103/PhysRevLett.118.154802

[17] D. Cesar *et al.*, "Ultrafast gating of a mid-infrared laser pulse by a sub-pC relativistic electron beam", *J. Appl. Phys.*, vol. 118, p. 234506, 2015. doi:10.1063/1.4937401

[18] Poisson Superfish, http://laacg.lanl.gov/laacg/services/download_sf.phtml

[19] Ansys, http://www.ansys.com

[20] V. Dolgashev, "High Magnetic Fields in Couplers of X-Band Accelerating Structures", in *Proc. Particle Accelerator Conf. (PAC'03)*, Portland, Oregon, USA, 2003, pp. 1267–1269.

[21] D. T. Palmer *et al.*, "Microwave Measurements of the BNL/SLAC/UCLA 1.6 Cell Photocathode RF Gun", in *Proc. Particle Accelerator Conf. (PAC'95)*, Dallas, Texas, USA, 1995, pp. 982–984.

[22] X. Guan *et al.*, "Study of RF-asymmetry in photo-injector", *Nucl. Instrum. Methods Phys. Res. Sect. A*, vol. 574, no. 1, p. 17, 2007. doi:10.1016/j.nima.2007.01.088

[23] M. S. Chae *et al.*, "Emittance growth due to multipole transverse magnetic modes in an rf gun", *Phys. Rev. ST Accel. Beams*, vol. 14, no. 10, p. 104203, 2011. doi:10.1103/PhysRevSTAB.14.104203

[24] COMEB, http://www.comeb.it

[25] L. C. Maier *et al.*, "Field strength measurement in resonant cavities", *J. Appl. Phys.*, vol. 23, no. 1, pp. 68–77, 1952. doi:10.1063/1.1701980

[26] Research Instruments, http://research-instruments.de

[27] A. Grudiev *et al.*, "Design of an X-Band Accelerating Structure for the CLIC Main Linac", in *Proc. 24th Linear Accelerator Conf. (LINAC'08)*, Victoria, BC, Canada, 2008, paper THP062, pp. 933–935.

[28] D. Alesini *et al.*, "The C-Band accelerating structures for SPARC photoinjector energy upgrade", *J. Inst.*, vol. 8, no. 5, p. P05004, 2013. doi:10.1088/1748-0221/8/05/P05004

[29] D. Alesini *et al.*, "Tuning procedure for traveling wave structures and its application to the C-Band cavities for SPARC photo injector energy upgrade", *J. Inst.*, vol. 8, no. 10, p. P10010, 2013. doi:10.1088/1748-0221/8/10/P10010

[30] D. Alesini *et al.*, "Design, realization and test of C-band accelerating structures for the SPARC_LAB linac energy upgrade", *Nucl. Instrum. Methods Phys. Res. Sect. A*, vol. 837, pp. 161–170, 2016. doi:10.1016/j.nima.2016.09.010

[31] Instrumentation Technologies, http://www.i-tech.si

[32] L. Piersanti *et al.* "Review of the ELI-NP-GBS Low Level RF and Synchronization Systems", in *Proc. 9th Int. Particle Accelerator Conf. (IPAC'18)*, Vancouver, BC, Canada, Apr-May 2018, pp. 2162–2165. doi:10.18429/JACoW-IPAC2018-WEPAL010

[33] Menlo Systems, http://www.menlosystems.com

[34] H. Kogelnick *et al.*, *Appl. Opt.*, vol. 5, p. 1550, 1966.

[35] T. Omori *et al.*, *Nucl. Instrum. Methods Phys. Res., Sect. A*, vol. 500, pp. 232–252, 2003. doi:10.1016/S0168-9002(02)01985-X

[36] A. J. Rollason *et al.*, *Nucl. Instrum. Methods Phys. Res., Sect. A*, vol. 526, pp. 560–571, 2004. doi:10.1016/j.nima.2004.02.017

[37] I. Yamane *et al.*, in *Proc. 1st Int. Particle Accelerator Conf. (IPAC10)*, Kyoto, Japan, 2010, pp. 1402–1404.

[38] K. Dupraz *et al.*, "Design of a polarized positron source for linear colliders", emphPhys. Rev. ST Accel. Beams, vol. 17, p. 033501, 2014. doi:10.1103/PhysRevSTAB.17.033501

[39] K. Cassou *et al.*, "Laser Beam Circulator for the Generation of a High Brilliance Gamma Beam at ELI-NP", in *Proc. High Intensity Lasers and High Field Phenomena 2018*, Strasbourg, France, 2018. doi:10.1364/HILAS.2018.HW4A.7

[40] Alsyom Alcen, https://www.alsyom-alcen.com